CC BY

Slow build-up of turbidity currents triggered by a moderate earthquake in the Sea of Marmara

Pierre Henry[1], M Sinan Özeren[2], Nurettin Yakupoğlu[3], Ziyadin Çakir[3], Emmanuel de Saint-Léger[4], Olivier Desprez de Gésincourt[4], Anders Tengberg[5], Cristele Chevalier[6], Christos Papoutsellis[1], Nazmi Postacıoğlu[7], Uğur Dogan[8], Hayrullah Karabulut[9], Gülsen Uçarkuş[3], M Namık Çağatay[3]

[1]Aix Marseille Univ, CNRS, IRD, INRAE, Coll France, CEREGE, Aix-en-Provence, France, [2]Istanbul Technical University, Eurasia Institute of Earth Sciences, Maslak, Istanbul, Turkey, [3]Istanbul Technical University, Geological Engineering Dept., Maslak, Istanbul, Turkey, [4]CNRS, DT INSU, Parc national d'instrumentation océanographique, Plouzané, France, [5]Aanderaa Data Instruments AS, Bergen, Norway, [6]Aix Marseille Univ, CNRS, IRD, MIO, Aix-en-Provence, France, [7]Istanbul Technical University, Physics Dept., Maslak, Istanbul, Turkey, [8]Yıldız Technical University, Geomatic Engineering Dept., Istanbul, Turkey, [9]Bogazici University, KOERI, Istanbul, Turkey

Abstract. Earthquake-induced submarine slope destabilization is known to cause debris flows and turbidity currents but data on the deep-sea hydrodynamic events following earthquakes are limited. An instrumented frame deployed at the seafloor in the Sea of Marmara Central Basin near the outlet of a canyon recorded some consequences of a M_W=5.8 earthquake that occurred Sept 26, 2019 without causing any significant tsunami. The hypocenter was located 10-12 km beneath the canyon, 5 km ENE of the device. The instrumentation comprises a pressure recorder and a 1.9-2 MHz Doppler recording current meter set 1.5 m above the seafloor. The records show that even a moderate earthquake can trigger a complex response involving mud flows and turbidity currents. We infer simultaneous slope failures at various locations producing complex current patterns and causing build-up of kinetic energy over several hours. This implies caution should be taken in marine paleoseismology when attempting to tie seismoturbidites with large earthquakes of historical importance.

CC BY

1. Introduction

Triggering of mass flows and turbidity currents by earthquakes is a hazard that can damage infrastructure at the seafloor (Heezen et al., 1954) and may enhance co-seismic tsunami generation (Okal and Synolakis, 2001; Synolakis et al., 2002; Hebert et al., 2005; Ozeren et al., 2010). It is often considered that a peak ground acceleration (PGA) of the order of 0.1 g is needed for an earthquake to trigger a submarine slope instability (Dan et al., 2008; Nakajima and Kanai, 2000). However, a global compilation of cable breaks shows that, exceptionally, mass flow have been triggered by individual earthquakes of M_w as low as 3.1 (with PGA $\approx 10^{-3}$ g) and that, on the other hand many M_w>7 have failed to break cables, notably in zones (e.g. Japan Trench) where sediment input is relatively low and earthquakes frequent (Pope et al., 2016). In the Mediterranean region, the threshold is reportedly around M_w = 5.

In spite of this high regional variability, turbidite deposits in several seismically active zones have been used successfully as paleoseimological event markers (Goldfinger et al., 2003, 2012; McHugh et al., 2014; Ikehara et al., 2016). This requires distinguishing between seismoturbidites, caused by earthquakes and related mass wasting events, from those resulting from other processes (e.g. floods, storms, sediment loading). Seismoturbidites are generally described as turbidite-homogenites where a basal silt-sand bearing layer is overlaid by a layer of apparently homogenous mud with small or gradual, if any, variations in grain size and chemical composition (Polonia et al., 2013; McHugh et al., 2011; Çağatay et al. 2012; Eriş et al., 2012; Gutierrez-Pastor et al., 2013; Beck et al., 2007). In lakes and closed basins several characteristics of deposits following earthquake or landslides, such as the sharp boundary between turbidite and homogenite layers, the alternation of silt/sand and mud laminae within a single turbidite-homogenite unit and presence of bi-directional cross- or flaser- bedding have been interpreted as indicators of deposition from oscillatory currents associated with seiches or turbidity current reflection (Beck et al., 2007; Çağatay et al. 2012; McHugh et al., 2011). Seismoturbidites on ocean margins have fairly similar characteristics to those in closed basins but their layering has been interpreted differently, as a consequence of confluence (stacked or amalgamated turbidites) or current speed variations (multi-pulsed turbidites) (Gutierrez-Pastor et al., 2013; Nakajima and Kanai, 2000; Goldfinger et al., 2003). There is currently a lack of in situ records that could substantiate inferred hydrodynamic processes. Monitoring

CC BY

experiments brought records of representative cases of turbidity currents flowing in submarine canyons and initiated by meteorological events and occasionally by landslides (Azpiroz-Zabala et al., 2017; Khripounoff et al., 2012; Xu et al., 2004, 2010; Liu et al., 2012; Hughes Clarke, 2016). Oscillatory currents resulting from internal waves have been recorded after landslides in lakes (Brizuela et al., 2019). On the other hand, most information on earthquake-triggered events is still indirect based on cable ruptures (e.g. Pope, 2017; Hsu et al., 2008), combined with geomorphological and sedimentological observations (Cattaneo et al., 2012; Piper et al., 1999), and information from displaced instruments (Garfield et al., 1994). In Japan, in situ records of pressure and temperature were obtained from displaced OBSs after the Tohoku 2011 earthquake (Arai et., 2013) and ADCP data from a cabled observatory after the Tokachi-Oki 2003 earthquake (Mikada et al., 2006). In both cases strong currents of more than 1 m/s were implied starting 2-3 hours after the earthquake with no indication of oscillation or pulsing.

We here present results from an instrumental deployment at the seafloor that accidentally recorded the consequences of an earthquake of Mw = 5.8, which occurred 09/26/2019 in the Sea of Marmara (Figure 1A). Holocene seismoturbidite records in the Sea of Marmara basins display a recurrence of 200 to 300 years, that roughly corresponds to the recurrence interval of Mw>7 earthquakes (McHugh et al., 2006, 2014; Drab et al., 2012, 2015; Yakupoğlu et al., 2018; Bulut et al., 2019). The pressure, temperature and current record from this single instrument demonstrate that this moderate earthquake triggered turbidity currents. However, the instrument suffered a rather complex sequence of disturbances and a 10 hours delay is observed between the earthquake and the recording of peak current. We here propose a scenario which could explain the observations and discuss their implications for the understanding of seismoturbidite records.

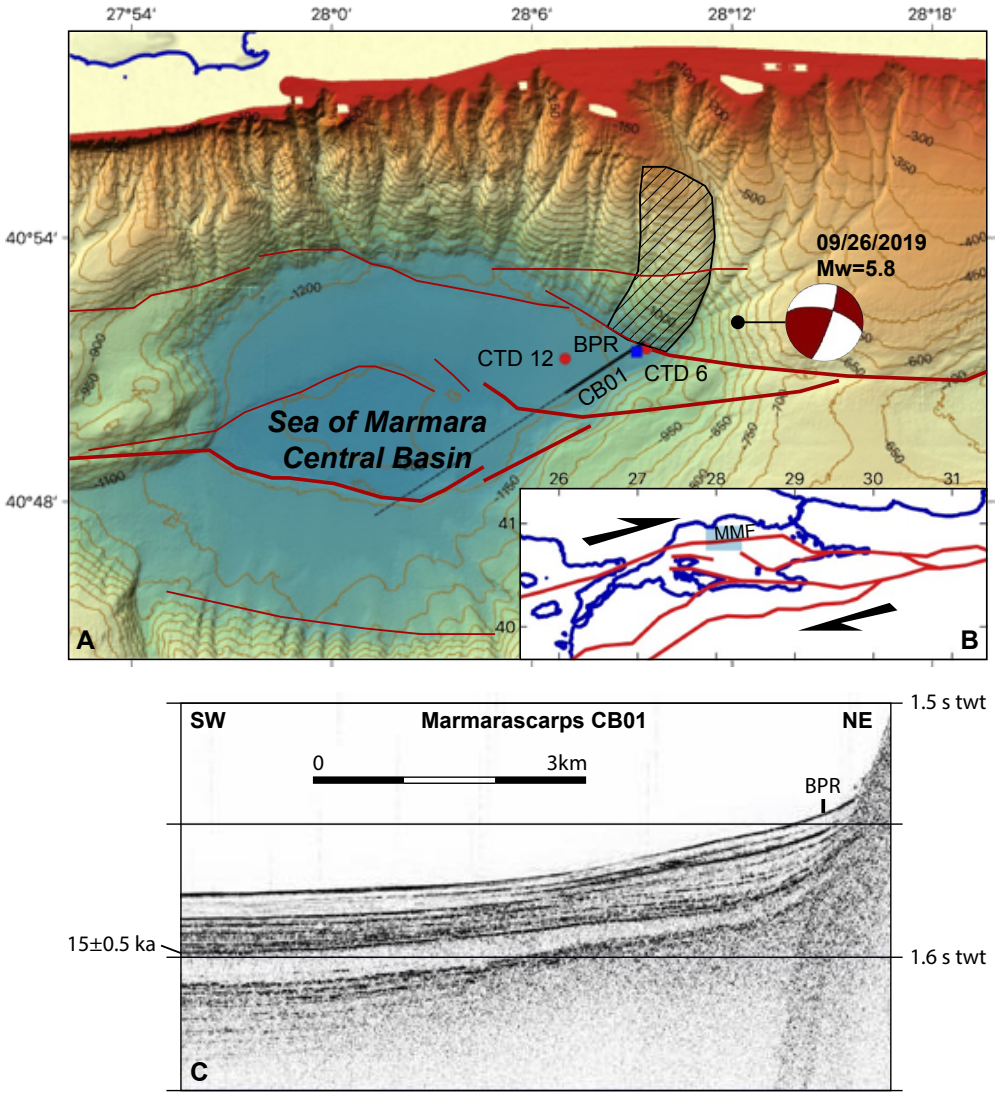

Figure 1. Context of instrumental deployment. (**A**) bathymetric map of the Sea of Marmara Central Basin with simplified fault geometry (in red). The hatched zone is a suspected mass wasting zone (Zitter et al., 2012). Location of instrumented frame comprising bottom pressure recorder (BPR) and doppler current meter is indicated by blue square. Red dots are CTD profiles 6 and 12 shown in supplementary material S1. Epicenter location and focal mechanism of recorded earthquake is indicated. (**B**) Location of study area. North Anatolian Fault system is shown in red. MMF is the Main Marmara Fault. (**C**) Sediment sounder profile from Marmarascarps cruise (Armijo and Malavieille, 2002). Indicative age of reflector from Beck et al. (2007). The instrument (BPR) was deployed on a depositional fan at the base of slope and canyon outlet that differ in character from the hemipelagite / turbidite-homogenite sequence in the basin.

CC BY

Context and data collection

A series of instrumental deployments was planned to record naturally occurring resonant water column oscillations (seiches) at various locations in the Sea of Marmara with the aim to improve tsunami models. An instrumented frame was thus deployed at 40.8568° N, 28.1523° E and 1184 m water depth in the Central Basin on May 9, 2019 and recovered 6 months later (11/19/2019)(Figure 1A). This site is located at the outlet of a branched canyon system originating from the edge of the continental shelf (Figure 1). Sediment sounder profiles indicate a depositional fan or lobe is present at this location (Figure 1C). The short canyons observed on the relatively steep sedimented slope (≈10°) of the Sea of Marmara deep basins are presumably fed by instabilities of the canyon heads and walls (Zitter et al. 2012; Çağatay et al., 2015). In addition, the slope west of the canyons immediately north of the deployment site hosts a mass wasting feature covering about 24 km^2 (Zitter et al. 2012). The Main Marmara Fault (MMF, Figure 1B), is defined as the part of the northern branch of the North Anatolian Fault system crossing the Sea of Marmara (Le Pichon et al., 2001, 2003). A splay of the MMF runs along the base of this slope (Armijo et al., 2002; Grall et al., 2012; Sengor et al., 2014). The 09/26/2019 earthquake occurred beneath the canyon system and its epicenter is located 5 km ENE of the instrument (Figure 1). The rupture occurred within the crust at 9-13 km depth on a northward dipping fault located north of principal displacement zone of the Main Marmara Fault. The focal mechanism and aftershock distribution indicate right-lateral strike-slip with a reverse component (Karabulut et al., 2020). The rupture did not reach the seafloor, nor caused a tsunami. For instance, tidal gauge records obtained at Marmara Ereglisi do not deviate more than 1hPa from the local tidal model. A M_w = 4.7 foreshock occurred two days before at 8:00:24 on 24/09/2019 within 500 m of the main shock.

As we will show that the 09/26/2019 earthquake caused the instrumented device to lay on its side for several hours and then straighten up, understanding the setup of the seafloor device and its stability has some importance (Figure 2A). The frame is made of aluminium and has 6 rigidly bound flotation spheres of 25 daN buoyancy each. The net weight of the instrumented frame in water is -80 daN. The frame is rigidly attached to a 12-cm-thick 1.5x1.3 m concrete slab, weighting 300 daN in water. The

CC BY

assembly of the heavy slab and buoyant frame is stable in upright position in the water and on the seafloor. If some external forces cause the assembly to tilt and lay on one side, the moment of the gravity and buoyancy forces should straighten the device back to upright position when these external forces are removed.

The instrumentation on the frame comprises (1) an RBR bottom pressure recorder (BPR) with a Paroscientific 0-2000 m Digiquartz sensor, (2) a Seaguard recording current meter (RCM) equipped with a Z-pulse 4520 Doppler current meter operating in the 1.9-2 MHz frequency range and other sensors: temperature, pressure (tide sensor Aandera 5217), conductivity, oxygen (Aandera optode) (Figure 2). The RBR pressure recording interval was set to 5s and that of the Seaguard RCM to one hour for all sensors. The Doppler current meter worked in burst mode, averaging 150 pings taken every second at the end of each one-hour recording interval. The Z-pulse sensor was set on the upper part of the frame 1.5 m above the seafloor and emit 4 narrow (2°) beams at orthogonal directions in a plane, parallel to the seafloor if the frame is standing upright, and measures Doppler backscatter in cells extending 0.5-to-2 meters from the instrument (Figure 2B). The instrument was set in forward ping mode, so that only data from sensors measuring a positive Doppler shift (current toward the instrument) is recorded. The tide sensor is a piezoresistive sensor of accuracy comparable to that of the Digiquartz sensors (4kPa for a 0-2000 m sensor vs. 2kPa for a Digiquartz sensor with the same range) and 0.2 hPa (2 mm) resolution and comprises a temperature sensor of 0.2°C accuracy and 0.001°C resolution. The tide sensor averages pressure measured at a 2 Hz sampling rate over 300 s.

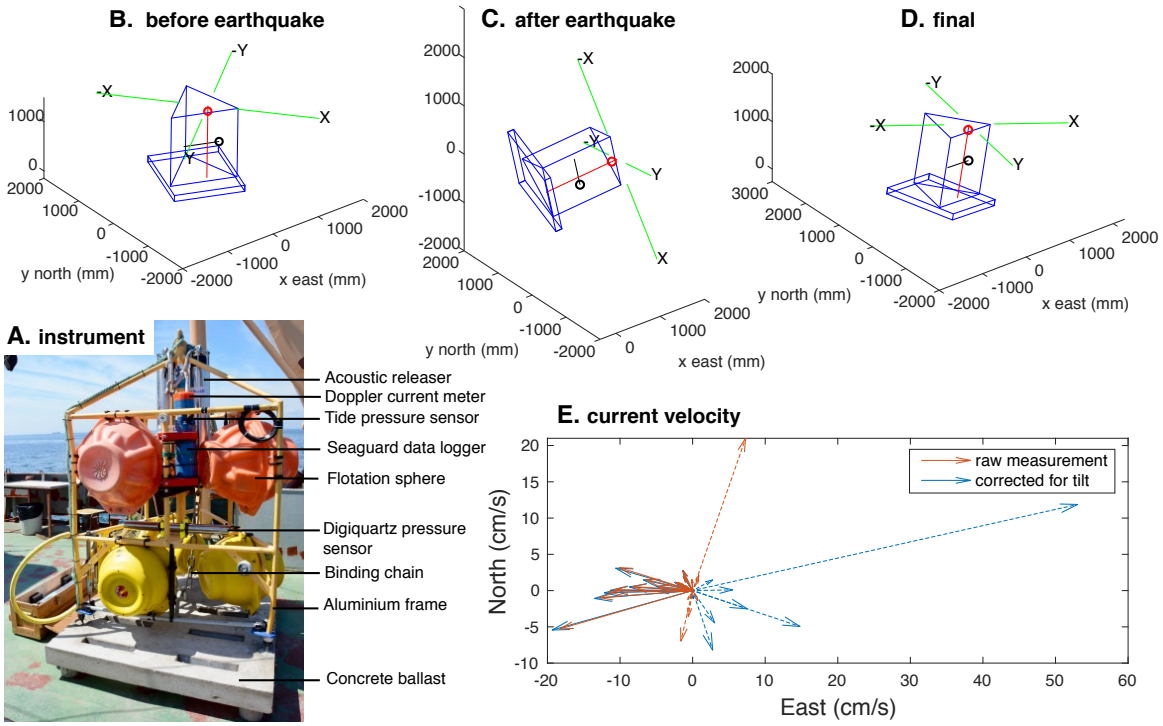

Figure 2. Instrumented frame. (A) photo of the instrumented frame before deployment. Reconstruction of frame position based on instrument tilt-meter and compass data: (B) before the earthquake; (C) Tilted, between, 25 minutes and 10 hours after earthquake; (D) back in nearly upright position 11.5 hours after earthquake. Position of Digiquartz pressure sensor (black circle), Aandera tide sensor (red circle) and Doppler current meter beam cells (green segments) (E) Current velocity arrows recorded every hour between 12:00 09/26/2019 and 06:00 09/27.2019. Dashed arrows show measurements acquired when the instrument was tilted in position C, plain arrows when it was back in upright position D.

2. Results and interpretations

2.1. Pressure and tilt records

The seismic wave train from the earthquake is recorded by the Digiquartz pressure sensor as oscillations, initiated by a pressure drop of 65 hPa between 10:59:22 and 10:59:26 (Figure 3A). Pressure sensors are sensitive to pressure variations caused by P-waves and Digiquartz sensors are also intrinsically sensitive to acceleration, but to a small extent, 160 hPa/g for an instrument with 20 MPa range according to the calibration report. For the sampling interval of 5s used in this setup,

CC BY

the recorded signal is aliased, which precludes quantitative interpretation in term of velocity or acceleration. However, the initial pressure drop may indicate a negative polarity of the first P arrival at the instrument site, located on an ascending ray-path.

Twenty-five minutes after the earthquake, a new disturbance of the pressure sensor is observed at 11:23:41. The pressure then progressively increases by 30.9 hPa in 15 seconds between 11:24:46 and 11:25:01 before stabilizing. Over the corresponding one-hour-time-interval between successive records, the Seaguard RCM, initially subvertical (tilt less than 2°), acquires a strong tilt (Figure 2B). At 11:57:48, measured tilt is -65° along the X-axis and +19° along the Y-axis, with X-axis in a N161° azimuth and these values remain constant ±2° over the next 10 hours, corresponding to an absolute tilt of 68° (Figure 3B). The tilting of the instrument causes the Digiquartz and Tide sensors to record different pressure variations because they are located at different positions on the frame (figure). Moreover, the pressure readings by the Digiquartz sensor also depend on its orientation relative to Earth gravity. Pressure at the Tide sensor location increases about 100 kPa, corresponding to a 1 m drop and indicating that the frame was then practically laying on its side. Ten hours later, the device apparently straightens itself in about 5 seconds, between 21:28:29 and 21:28:34 as indicated by a rapid pressure variation. After that, the recorded tilt parameters are moderate and stabilize at -11.5° for the X-axis and 5.3° for the Y-axis, with X-axis in a N105.3° azimuth.

2.2. Current record and possible causes of tilting

During the 10 hours period when the instrument remained strongly tilted, it recorded currents varying both in speed and orientation but some precautions are needed when interpreting these data. The current component measured by transducers along the Y-axis, oriented N200°, probably remained accurate as the tilt along this axis is less than 20° and the measurement cell remained above the bottom (Figure 2B). On the other hand, the X-component may not be reliable. Because the sensor in the X direction is facing the seafloor, currents coming from this direction, and thus flowing northwestward will not be detected. However, data indicate that both current direction and speed varied during this time interval and the current measured along the Y-axis changed sign several times (Figure 2). Assuming raw measurement and tilt corrected measurements bracket the true current speed, four current pulses

CC BY

occurred, ranging from 5 cm/s to about 50 cm/s, the last one being the strongest (Figure 3B). The current speed in the first 2 hours after the earthquake apparently remained low, at most 5-6 cm/s. It is thus unlikely that the tilt of the device was caused by strong currents. Some short burst of current may have been missed because of the 1 hour sampling interval, but this would not explain why the frame then remained stable in a tilted position for several hours. Local liquefaction of the sediment beneath the device is also an unlikely cause because the tilting of the instrument occurred 25 minutes after the earthquake. A mud flow originating from the basin slopes thus appears as a more likely cause. This hypothesis would also acount for the presence of sandy mud caked on the device in various places : on the frame feet, on the acoustic releasers, on the optode connector, and also inside the plastic protection of a flotation sphere, from which bindings were broken and had to be repaired. On the other hand, the current speed in the 20-50 cm/s range recorded before, as well as after, the time when the device straightened up is strong enough to cause erosion of mud or sand deposits. It may thus be hypothesized that erosion freed the device from the mud cover. The flotation spheres on the frame and the concrete ballast at its base exert a moment that should keep the assembly stable in an upright position unless the frame is loaded with sediment. Once the device got back in an upright position, it recorded a current consistently flowing westward and progressively decreasing from 20 cm/s to background level (2 cm/s) in 9 hours (Figure 2E).

2.3. Acoustic backscatter record

The strength of the backscattered signal can be used as a proxy for turbidity. The Seaguard RCM emits in the 1.9-2 MHz band corresponding to a wavelength (λ) of 750 µm. Doppler backscatter current meters have maximum sensitivity for particles of diameter $D = \lambda/\pi$ and can detect particles down to diameter $D = 0.08\ \lambda$, for which backscatter power is less than 1/10 of peak backscatter power (Guerrero et al., 2011, 2012). The seaguard RCM should thus be mostly sensitive to the presence in suspension of sand size particles (more than 63 µm). The background backscatter amplitude level is -40dB before the earthquakes and increases to the -20 dB to -13 dB range after the earthquake (Figure 3C), which implies sand sized sediment was put in suspension soon after the earthquake although the local current speed remained relatively low (about 5 cm/s at most). After the device went back to near vertical position,

CC BY

signal strengh reaches a maximum of -7.6 dB, which correspond to an amplitude ratio of 42 and an intensity ratio of 1800 compared to base level. Similar signal strength levels are typically reached with the Z-Pulse sensor in highly turbid water such as in estuaries. During deep sea deployments signal strength range more typically between -60 and -40 dB. After reaching peak value, backscattered signal strengh progressively decays to background levels in 3 days (Figure 3C).

2.4. Temperature record

The recorded temperature decreases progressively by about 0.015°C after the first hydrologic disturbance and tilting of the instrument until the recorded current reaches its maximum value (Figure 3C). Temperature then progressively increases to reach nearly the same value as before the event. The Sea of Marmara is stratified, with a low salinity (20-22‰) 20-30 m surface layer that displays strong seasonal temperature variability overlaying a high salinity (about 38‰) body of seawater at 14-15°C derived from the Aegean Sea (Beşiktepe et al., 1994)(supplementary material S1). Only a very small variation in temperature recorded indicates that the turbid water originates from the deep-water body. Within this body, the potential temperature generally decreases with depth, which would in principle imply that a turbidity current, flowing downward, should cause a small temperature increase. However, the deployment site is prone to seasonal cascading, so that the initial temperature structure may have been disturbed. Example of CTD profiles recorded in June 2007 (Henry et al., 2007) are given in the supplementary material S1. No CTD profile is available in Sept 2019, but variations in temperature and oxygen concentration associated with mild currents (<5 cm/s) were recorded by the instrument in May-July 2019, and again Sept 20. It follows that the slight temperature decrease observed after the earthquake can result from the mixing of a warmer bottom water layer with the bulk of the deep-water layer. However, the observation of a temperature drop precludes that the turbid water originates from depths less than 400 m, as water present between 400 m and the halocline is at a higher temperature than the deeper water throughout the year (Beşiktepe et al., 1994).

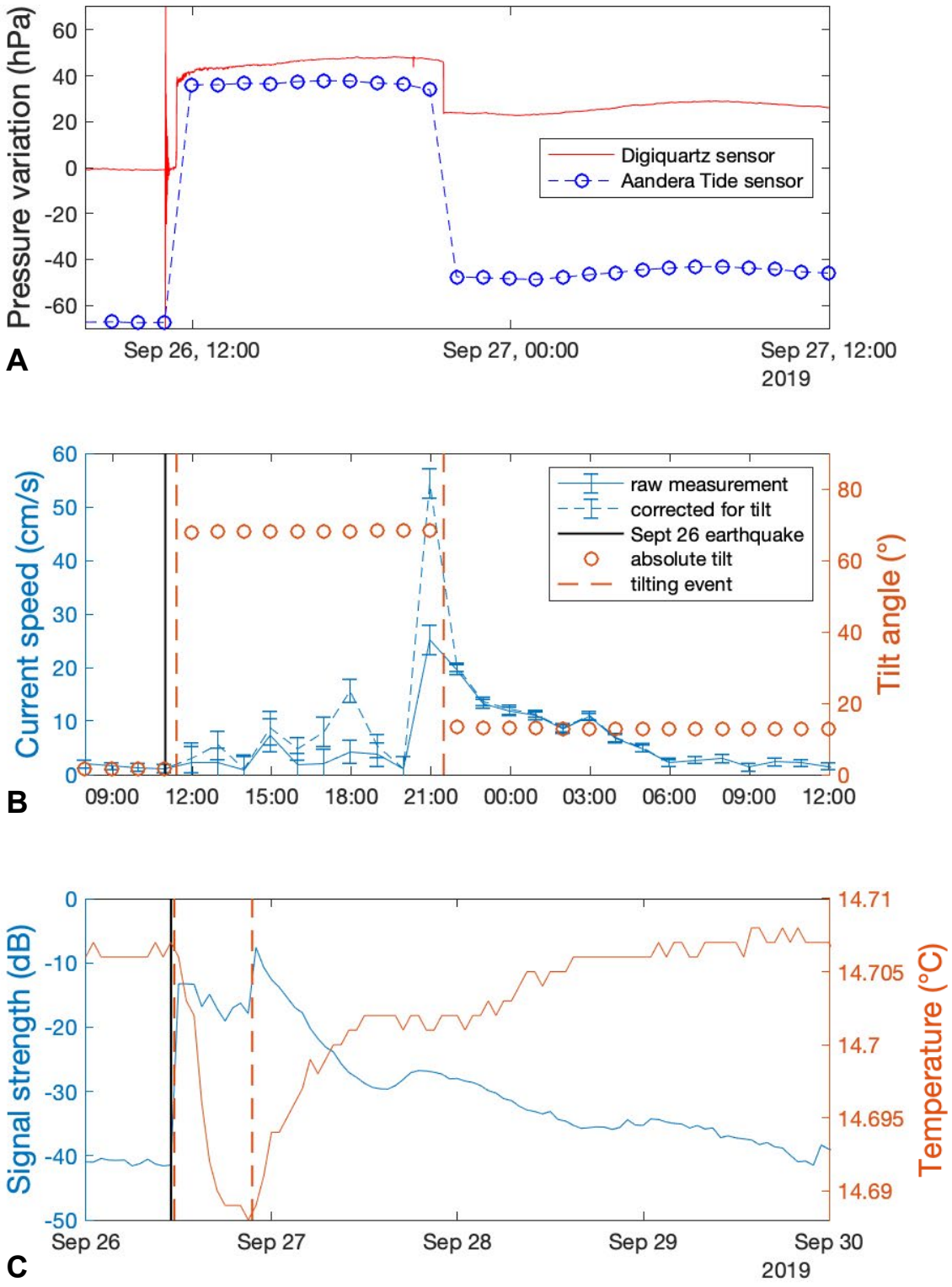

Figure 3. Time series of (A) pressure variations recorded by two instruments on the instrumented frame. (B) current and tilt data recorded by Seaguard RCM. (C) Backscatter signal strength and temperature variations recorded by Seaguard RCM.

CC BY

2.5. Inferred sequence of events

These observations provide some insight on the complex sequence of events that followed the earthquake and suggest the following scenario. After the passing of the seismic wave, triggering of instability on slopes adjacent to the deployment site caused mud flows that spread on the basin floor causing the tilting of the instrument 25 minutes after the earthquake and bottom water turbidity. The base of the nearest slope is about 400 m north of the instrument. This would imply a minimum velocity of 20 cm/s for the mudflow to reach the device location in 25 minutes. During the following 10 hours, successive current pulses with variable directions tend to increase in strength over time. Widespread slope instabilities triggered by the earthquake may have resulted in several turbidity currents recorded as succesive pulses with variable directions. The role of seiches and surface gravity waves in sediment resuspension can be ruled out as no tsunami was recorded by near shore tidal gauges around the Sea of Marmara. The relationship between long period gravity wave amplitude A and bottom current amplitude U in the shallow water approximation is given by $U=(g/H)^{1/2}A$, where H is water column height. An oscillatory current of 10 cm/s at 1200 m depth would thus correspond to a free surface oscillation of 1 m (or 100 hPa) for a standing wave (seiche) as well as a progressive wave (tsunami). This should have been easily detected in a sea where tidal amplitude is about 10 cm (Alpar and Yüce, 1998). The influence of baroclinic internal waves on the halocline at 20-30 m depth must also be ruled out as they cannot physically produce currents of more than a few cm/s at 1200 m. It still remains possible that the interface at the top of the turbid cloud is affected by baroclinic waves. On the other hand, current pulses increase in strength over time, which suggests that turbidity currents initiated further upslope may have reached the site after a longer delay but may also have gained more kinetic energy on their downhill path. The last pulse, reaching a speed of the order of 50 cm/s apparently caused enough erosion to free the device from the mud accumulation. The current then stabilizes in a westward direction and decays progressively over the next 9 hours, which suggests the tail of a turbidity current flowing in the canyon E of the deployment site has been recorded. The hours-long delay between the earthquake and the passing of the fastest current over the instrument may hypothetically correspond to the time for the head of the turbidity current to travel from its source to the location of the instrument. The length of the canyon valley between the device location and the 400 m isobath, inferred to be the minimum depth of the turbid water source, is about 13 km. In this

CC BY

scenario, the average velocity of the head of the turbidity current would be 30-40 cm/s. Alternatively, a sequence of slope failures may have lasted up to several hours after the earthquake. The decay of the backscatter signal strength over the next 3 days may reflect the settling of sand size particles put in suspension in the water column after this sequence of events. For a first order assessment, Stokes settling velocity, an upper bound valid in dilute suspensions (e.g. Guazelli and Morris, 2012) may be used. The Stokes settling velocity of 63 µm quartz grains (density 2650 kg/m^3) in 13°C seawater is 2.7 mm/s, allowing such grains to drop by a maximum of 700 m in 3 days.

3. Discussion and conclusion

The data obtained with this seafloor device may be compared with more complete records of turbidity currents obtained elsewhere with ADCP deployments and/or water column mooring lines. The duration of the event in the Sea of Marmara (about 10 hours) appear fairly typical and comparable with events recorded in other locations regardless of the initiation mechanism, which comprise hyperpycnal flows from river floods (Var and Gaoping canyons), storm waves and dredging (Monterey canyon) and slope instabilities triggered by an earthquake (Tokachi-oki) or by other processes (Var canyon) (Khripounoff et al., 2012; Xu et al., 2004; Liu et al., 2012; Mikada et al., 2006). Longer duration events with very different hydrodynamic characteristics have been observed in larger scale systems (e.g. Congo deep sea canyon, Azpiroz-Zabala et al., 2017). On the other hand, events recorded closer to shore on the edge of the continental shelf or on a delta front have much shorter durations (Xu et al., 2010; Hughes Clarke, 2016). In events of comparable scale to the Sea of Marmara one, the velocity of the current generally reaches its maximum several meters above the seafloor, so that the velocity recorded by our instrument at 1.5 m from the seafloor is within the boundary layer, and lower that either the maximum current velocity of the velocity of the head of the turbidity current. A velocity of several tens of centimeter per second is representative of the slower recorded examples, corresponding to mud rich flows associated with hyperpycnal flows or to the smaller landslides. Turbidites following large earthquakes or large slope instabilities have reached maximum velocities of 20 m/s (Piper et al., 1999) and 2-7 m/s was reported for the Tohoku turbidity current (Arai et al., 2013).

CC BY

The 10 hours delay observed in the Sea of Marmara between the triggering event and the peak of the turbidity current is long compared to the 2 hours delay observed after Tohoku and Tokachi-oki earthquakes. We suggested earlier that the long delay may simply result from a slower velocity of the turbidity current or from delayed slope failure. Another possibility is delayed ignition, which may occur if the turbidity current develops indirectly from the hydrodynamic instability of a turbid cloud resulting from slope failures and/or ground shaking rather than by progressive acceleration of a dense mud flow (Parker, 1982; Mulder and Cochonnat, 1996; Piper and Normark, 2009).

The scenario we propose for the Sept 26, 2019 earthquake involving mud flows from proximal sources, followed by turbidity currents originating at larger distances, and the subsequent settling of sediment in suspension, could relate with the structure of turbidite-homogenites. Progressive or pulsed build-up of turbidity current energy is considered typical of hyperpycnal flows initiated by river floods (Mulder et al., 2003) but reverse grading and pulsing is also observed in seismoturbidites (Gutierrez-Pastor et al., 2013). In the Sea of Marmara, many of the laminated turbidites sampled in Kumburgaz Basin formed from the amalgamation (below the homogenite layer) of at least two flows, the first one being finer and less sorted (Yakupoğlu et al., 2019). The coarsening observed in this context is often associated with an increase of the calcium content indicative of a shallower source, rich in biogenic carbonate material. The geomorphological context of the deployment site south of a slope identified as unstable from geomorphological criteria and on a depositional fan at the outlet of a canyon is also consistent with this scenario (Zitter et al., 2012). However, it is still unknown whether the Sept 26 event left a trace on the seafloor morphology and in the sediment record. If such a moderate earthquake is indeed associated with a turbidite-homogenite deposit, it may be wrong to associate each seismoturbidite with a major historical earthquake. Performing new core sampling and very high-resolution geophysical surveys in the Central Basin would thus have important implications for the understanding of seismoturbidite records and for the assessment of geohazards.

Acknowledgements

Financial support was provided by the bilateral ANR/TÜBITAK collaborative research project MAREGAMI (ANR-16-CE03-0010-02 and Tübitak Project 116Y371) and by

CC BY

CNRS- INSU through the European Multidisciplinary Sea Observatory (EMSO) Research Infrastructure program. DT-INSU and Istanbul Technical University hydrodynamic engineering department provided technical support for device design, construction, and deployment. Bernard Mercier de Lépinay provided processed sediment sounder profiles. We thank the crew and Captain of R/V Yunus (Istanbul University) for their support during installation and recovery of the instruments. Data is available through OSU Pytheas ERDDAP server (Henry et al., 2019) and SISMER Oceanographic Data portal (http://en.data.ifremer.fr/SISMER)

Memo: 1 PU is 500 words or 1 display element (figure or table), Size limit 12 PU

References

Alpar, B., & Yüce, H. (1998). Sea-level variations and their interactions between the Black Sea nd the Aegean Sea. Estuarine, Coastal and Shelf Science, 46, 609–619.

Arai, K., Naruse, H., Miura, R., Kawamura, K., Hino, R., Ito, Y., Inazu, D., Yokokawa, M., Izumi, N., Murayama, M., & Kasaya, T. (2013). Tsunami-generated turbidity current of the 2011 Tohoku-Oki earthquake. Geology, 41(11), 1195–1198. https://doi.org/10.1130/G34777.1

Armijo, R., Meyer, B., Navarro, S., King, G., & Barka, A. (2002). Asymmetric slip partitioning in the Sea of Marmara pull-apart: a clue to propagation processes of the North Anatolian Fault? Terra Nova, 14(2), 80–86. https://doi.org/10.1046/j.1365-3121.2002.00397.x

Armijo, R. and J. Malavieille (2002) MARMARASCARPS cruise, RV L'Atalante, https://doi.org/10.17600/2010140

Azpiroz-Zabala, M., Cartigny, M. J. B., Talling, P. J., Parsons, D. R., Sumner, E. J., Clare, M. A., Simmons, S. M., Cooper, C., & Pope, E. L. (2017). Newly recognized turbidity current structure can explain prolonged flushing of submarine canyons. Science Advances, 3(10). https://doi.org/10.1126/sciadv.1700200

Beck, C., Mercier de Lépinay, B., Schneider, J. L., Cremer, M., Çağatay, N., Wendenbaum, E., et al. (2007). Late Quaternary co-seismic sedimentation in the Sea of Marmara's deep basins. Sedimentary Geology, 199, 65–89. https://doi.org/10.1016/j.sedgeo.2005.12.031

Beşiktepe, Ş. T., Sur, H. İ., Özsoy, E., Latif, M. A., Oğuz, T., & Ünlüata, Ü. (1994). The circulation and hydrography of the Marmara Sea. Progress in Oceanography, 34(4), 285–334. https://doi.org/10.1016/0079-6611(94)90018-3

CC BY

Brizuela, N., Filonov, A., & Alford, M. H. (2019). Internal tsunami waves transport sediment released by underwater landslides. Scientific Reports, 9(1), 10775. https://doi.org/10.1038/s41598-019-47080-0

Bulut, F., Aktuğ, B., Yaltırak, C., Doğru, A., & Özener, H. (2019). Magnitudes of future large earthquakes near Istanbul quantified from 1500 years of historical earthquakes, present-day microseismicity and GPS slip rates. Tectonophysics, 764(July 2018), 77–87. https://doi.org/10.1016/j.tecto.2019.05.005

Çağatay, M. N., Erel, L., Bellucci, L. G., Polonia, a., Gasperini, L., Eriş, K. K., Sancar, Ü., Biltekin, D., Uçarkuş, G., Ülgen, U. B., & Damci, E. (2012). Sedimentary earthquake records in the İzmit Gulf, Sea of Marmara, Turkey. Sedimentary Geology, 282, 347–359. https://doi.org/10.1016/j.sedgeo.2012.10.001

Çağatay, N. M., Ucarkus, G., Eris, K. K., Henry, P., Gasperini, L., & Polonia, A. (2015). Submarine canyons of the Sea of Marmara. In F. Briand (Ed.), Submarine Canyon Dynamics in the Mediterranean and Tributary Seas, CIESM Workshop Monograph n° 47 (pp. 123–135). CIESM Publisher, Monaco. https://doi.org/10.13140/RG.2.1.1692.8402

Cattaneo, A., Babonneau, N., Ratzov, G., Dan-Unterseh, G., Yelles, K., Bracane, R., Mercier De Lapinay, B., Boudiaf, A., & Daverchare, J. (2012). Searching for the seafloor signature of the 21 May 2003 Boumerdas earthquake offshore central Algeria. Natural Hazards and Earth System Science, 12(7), 2159–2172. https://doi.org/10.5194/nhess-12-2159-2012

Dan, G., Sultan, N., Savoye, B., Deverchere, J., & Yelles, K. (2009). Quantifying the role of sandy-silty sediments in generating slope failures during earthquakes: Example from the Algerian margin. International Journal of Earth Sciences, 98(4), 769–789. https://doi.org/10.1007/s00531-008-0373-5

Drab, L., Hubert Ferrari, A., Schmidt, S., & Martinez, P. (2012). The earthquake sedimentary record in the western part of the Sea of Marmara, Turkey. Natural Hazards and Earth System Science, 12(4), 1235–1254. https://doi.org/10.5194/nhess-12-1235-2012

Drab, L., Hubert‐Ferrari, A., Schmidt, S., Martinez, P., Carlut, J., & El Ouahabi, M. (2015). Submarine Earthquake History of the Çınarcık Segment of the North Anatolian Fault in the Marmara Sea, Turkey. Bulletin of the Seismological Society of America, 105(2A), 622–645. https://doi.org/10.1785/0120130083

Eriş, K. K., Çağatay, N., Beck, C., Mercier de Lepinay, B., & Corina, C. (2012). Late-Pleistocene to Holocene sedimentary fills of the Çinarcik Basin of the Sea of Marmara. Sedimentary Geology, 281, 151–165. https://doi.org/10.1016/j.sedgeo.2012.09.001

Garfield, N., Rago, T. A., Schnebele, K. J., & Collins, C. A. (1994). Evidence of a turbidity current in Monterey Submarine Canyon associated with the 1989 Loma Prieta

CC BY

earthquake. Continental Shelf Research, 14(6), 673–686. https://doi.org/10.1016/0278-4343(94)90112-0

Goldfinger, C., Nelson, C. H., & Johnson, J. E. (2003). Holocene earthquake records from the cascadia subduction zone and northern san andreas fault based on precise dating of offshore turbidites. Annual Review of Earth and Planetary Sciences, 31(1), 555–577. https://doi.org/10.1146/annurev.earth.31.100901.141246

Goldfinger, C., Nelson, C. H., Morey, A. E., Johnson, J. E., Patton, J., Karabanov, E., Gutiérrez-Pastor, J., Eriksson, A. T., Gràcia, E., Dunhill, G., Enkin, R. J., Dallimore, A., & Vallier, T. (2012). Earthquake Hazards of the Pacific Northwest Coastal and Marine Regions Turbidite Event History — Methods and Implications for Holocene Paleoseismicity of the Cascadia Subduction Zone Professional Paper 1661 – F. USGS, Professional Paper 1661-F, 170. Retrieved from http://pubs.usgs.gov/pppp1661f/

Grall, C., Henry, P., Tezcan, D., Mercier de Lepinay, B., Becel, A., Geli, L., Rudkiewicz, J.-L., Zitter, T., & Harmegnies, F. (2012). Heat flow in the Sea of Marmara Central Basin: Possible implications for the tectonic evolution of the North Anatolian fault. Geology, 40(1), 3–6. https://doi.org/10.1130/G32192.1

Guazzelli, E., Morris, J. F., & Pic, S. (2011). A Physical Introduction to Suspension Dynamics. Cambridge: Cambridge University Press. https://doi.org/10.1017/CBO9780511894671

Guerrero, M., Rüther, N., & Szupiany, R. N. (2012). Laboratory validation of acoustic Doppler current profiler (ADCP) techniques for suspended sediment investigations. Flow Measurement and Instrumentation, 23(1), 40–48. https://doi.org/10.1016/j.flowmeasinst.2011.10.003

Guerrero, M., Szupiany, R. N., & Amsler, M. (2011). Comparison of acoustic backscattering techniques for suspended sediments investigation. Flow Measurement and Instrumentation, 22(5), 392–401. https://doi.org/10.1016/j.flowmeasinst.2011.06.003

Gutiérrez-Pastor, J., Nelson, C. H., Goldfinger, C., & Escutia, C. (2013). Sedimentology of seismo-turbidites off the Cascadia and northern California active tectonic continental margins, northwest Pacific Ocean. Marine Geology, 336, 99–119. https://doi.org/10.1016/j.margeo.2012.11.010

Hébert, H., Schindelé, F., Altinok, Y., Alpar, B., & Gazioglu, C. (2005). Tsunami hazard in the Marmara Sea (Turkey): A numerical approach to discuss active faulting and impact on the Istanbul coastal areas. Marine Geology, 215, 23–43. https://doi.org/10.1016/j.margeo.2004.11.006

Heezen, B. C., Ericson, D. B., & Ewing, M. (1954). Further evidence for a turbidity current following the 1929 Grand banks earthquake. Deep Sea Research (1953), 1(4), 193–202. https://doi.org/10.1016/0146-6313(54)90001-5

CC BY

Henry, P., A.M.C. Şengör, M.N. Çağatay (2007) MARNAUT cruise, RV L'Atalante, https://doi.org/10.17600/7010070

Henry, P., Özeren, S., Libes M. (2019) Data access to EMSO / MAREGAMI Marmara, https://dataset.osupytheas.fr/geonetwork/srv/fre/catalog.search#/metadata/7175f88e-cde6-4a67-ada5-1e44a687156f

Hsu, S. K., Kuo, J., Lo, C. L., Tsai, C. H., Doo, W. Bin, Ku, C. Y., & Sibuet, J. C. (2008). Turbidity currents, submarine landslides and the 2006 Pingtung earthquake off SW Taiwan. Terrestrial, Atmospheric and Oceanic Sciences, 19(6), 767–772. https://doi.org/10.3319/TAO.2008.19.6.767(PT)

Hughes Clarke, J. E. (2016). First wide-angle view of channelized turbidity currents links migrating cyclic steps to flow characteristics. Nature Communications, 7(1), 11896. https://doi.org/10.1038/ncomms11896

Ikehara, K., Kanamatsu, T., Nagahashi, Y., Strasser, M., Fink, H., Usami, K., et al. (2016). Documenting large earthquakes similar to the 2011 Tohoku-oki earthquake from sediments deposited in the Japan Trench over the past 1500 years. Earth and Planetary Science Letters, 445, 48–56. doi:10.1016/j.epsl.2016.04.009

Karabulut, H., Guvercin, S., E., Eskikoy, F., Konca A. O., Ergintav, S. (2020). The moderate size septermber 2019 M_w 5.8 Silivri Earthquake unveils the complexity of the Main Marmara Fault shear zone, Submitted to Geophysical Journal International.

Khripounoff, A., Crassous, P., Lo Bue, N., Dennielou, B., & Silva Jacinto, R. (2012). Different types of sediment gravity flows detected in the Var submarine canyon (northwestern Mediterranean Sea). Progress in Oceanography, 106, 138–153. https://doi.org/10.1016/j.pocean.2012.09.001

Le Pichon, X., Chamot-Roooke, N., Rangin, C., & Sengör, A. M. C. (2003). The North Anatolian fault in the Sea of Marmara. Journal of Geophysical Research, 108, 2179. https://doi.org/10.1029/2002JB001862

Le Pichon, X., Şengör, A. M. C., Demirbağ, E., Rangin, C., İmren, C., Armijo, R., Görür, N., Çağatay, N., Mercier de Lepinay, B., Meyer, B., Saatçılar, R., & Tok, B. (2001). The active Main Marmara Fault. Earth and Planetary Science Letters, 192(4), 595–616. https://doi.org/10.1016/S0012-821X(01)00449-6

Liu, J. T., Wang, Y.-H., Yang, R. J., Hsu, R. T., Kao, S.-J., Lin, H.-L., & Kuo, F. H. (2012). Cyclone-induced hyperpycnal turbidity currents in a submarine canyon. Journal of Geophysical Research: Oceans, 117(C4), n/a-n/a. https://doi.org/10.1029/2011JC007630

McHugh, C. M. G., Seeber, L., Cormier, M. H., Dutton, J., Cagatay, N., Polonia, A., Ryan, W. B. F., & Gorur, N. (2006). Submarine earthquake geology along the North Anatolia Fault

CC BY

in the Marmara Sea, Turkey: A model for transform basin sedimentation. Earth and Planetary Science Letters, 248, 661–684. https://doi.org/10.1016/j.epsl.2006.05.038

McHugh, C. M., Seeber, L., Braudy, N., Cormier, M. H., Davis, M. B., Diebold, J. B., Dieudonne, N., Douilly, R., Gulick, S. P. S., Hornbach, M. J., Johnson, H. E., Mishkin, K. R., Sorlien, C. C., Steckler, M. S., Symithe, S. J., & Templeton, J. (2011). Offshore sedimentary effects of the 12 January 2010 Haiti earthquake. Geology, 39(8), 723–726. https://doi.org/10.1130/G31815.1

McHugh, C. M. G., Braudy, N., Çağatay, M. N., Sorlien, C., Cormier, M.-H., Seeber, L., & Henry, P. (2014). Seafloor fault ruptures along the North Anatolia Fault in the Marmara Sea, Turkey: Link with the adjacent basin turbidite record. Marine Geology, 353, 65–83. https://doi.org/10.1016/j.margeo.2014.03.005

Mikada, H., Mitsuzawa, K., Matsumoto, H., Watanabe, T., Morita, S., Otsuka, R., Sugioka, H., Baba, T., Araki, E., & Suyehiro, K. (2006). New discoveries in dynamics of an M8 earthquake-phenomena and their implications from the 2003 Tokachi-oki earthquake using a long term monitoring cabled observatory. Tectonophysics, 426(1–2), 95–105. https://doi.org/10.1016/j.tecto.2006.02.021

Mulder, T., & Cochonnat, P. (1996). Classification of Offshore Mass Movements. SEPM Journal of Sedimentary Research, Vol. 66. https://doi.org/10.1306/D42682AC-2B26-11D7-8648000102C1865D

Mulder, T., Syvitski, J. P. M., Migeon, S., Faugères, J.-C., & Savoye, B. (2003). Marine hyperpycnal flows: initiation, behavior and related deposits. A review. Marine and Petroleum Geology, 20(6–8), 861–882. https://doi.org/10.1016/j.marpetgeo.2003.01.003

Nakajima, T., & Kanai, Y. (2000). Sedimentary features of seismoturbidites triggered by the 1983 and older historical earthquakes in the eastern margin of the Japan Sea. Sedimentary Geology, 135(1–4), 1–19. https://doi.org/10.1016/S0037-0738(00)00059-2

Okal, E. A., & Synolakis, C. E. (2001). Comment on “Origin of the 17 July 1998 Papua New Guinea Tsunami: Earthquake or Landslide?” by E. L. Geist. Seismological Research Letters, 72(3), 362–366. https://doi.org/10.1785/gssrl.72.3.362

Özeren, M. S., Çağatay, M. N., Postacioğlu, N., Şengör, a. M. C., Görür, N., & Eriş, K. (2010). Mathematical modelling of a potential tsunami associated with a late glacial submarine landslide in the Sea of Marmara. Geo-Marine Letters, 30, 523–539. https://doi.org/10.1007/s00367-010-0191-1

Parker, G. (1982). Conditions for the ignition of catastrophically erosive turbidity currents. Marine Geology, 46(3–4), 307–327. https://doi.org/10.1016/0025-3227(82)90086-X

Piper, D. J. W., & Normark, W. R. (2009). Processes That Initiate Turbidity Currents and Their Influence on Turbidites: A Marine Geology Perspective. Journal of Sedimentary Research, 79(6), 347–362. https://doi.org/10.2110/jsr.2009.046

CC BY

Piper, D. J. W., Cochonat, P., & Morrison, M. L. (1999). The sequence of events around the epicentre of the 1929 Grand Banks earthquake: initiation of debris flows and turbidity current inferred from sidescan sonar. Sedimentology, 46(1), 79–97. https://doi.org/10.1046/j.1365-3091.1999.00204.x

Polonia, A., Vaiani, S. C., & De Lange, G. J. (2016). Did the A.D. 365 Crete earthquake/tsunami trigger synchronous giant turbidity currents in the Mediterranean Sea? Geology, 44(3), 191–194. https://doi.org/10.1130/G37486.1

Pope, E. L., Talling, P. J., & Carter, L. (2017). Which earthquakes trigger damaging submarine mass movements: Insights from a global record of submarine cable breaks? Marine Geology, 384, 131–146. https://doi.org/10.1016/j.margeo.2016.01.009

Şengör, A. M. C., Grall, C., İmren, C., Le Pichon, X., Görür, N., Henry, P., Karabulut, H., & Siyako, M. (2014). The geometry of the North Anatolian transform fault in the Sea of Marmara and its temporal evolution: implications for the development of intracontinental transform faults. Canadian Journal of Earth Sciences, 51(3), 222–242. https://doi.org/10.1139/cjes-2013-0160

Synolakis, C. E., Bardet, J.-P., Borrero, J. C., Davies, H. L., Okal, E. A., Silver, E. A., Sweet, S., & Tappin, D. R. (2002). The slump origin of the 1998 Papua New Guinea Tsunami. Proceedings of the Royal Society of London. Series A: Mathematical, Physical and Engineering Sciences, 458(2020), 763–789. https://doi.org/10.1098/rspa.2001.0915

Xu, J. P., Noble, M. A., & Rosenfeld, L. K. (2004). In-situ measurements of velocity structure within turbidity currents. Geophysical Research Letters, 31(9). https://doi.org/10.1029/2004GL019718

Xu, J. P., Swarzenski, P. W., Noble, M., & Li, A.-C. (2010). Event-driven sediment flux in Hueneme and Mugu submarine canyons, southern California. Marine Geology, 269(1–2), 74–88. https://doi.org/10.1016/j.margeo.2009.12.007

Yakupoğlu, N., Uçarkuş, G., Kadir Eriş, K., Henry, P., & Namık Çağatay, M. (2019). Sedimentological and geochemical evidence for seismoturbidite generation in the Kumburgaz Basin, Sea of Marmara: Implications for earthquake recurrence along the Central High Segment of the North Anatolian Fault. Sedimentary Geology, 380, 31–44. https://doi.org/10.1016/j.sedgeo.2018.11.002

Zitter, T. A. C., Grall, C., Henry, P., Özeren, M. S., Çağatay, M. N., Şengör, A. M. C., Gasperini, L., de Lépinay, B. M., & Géli, L. (2012). Distribution, morphology and triggers of submarine mass wasting in the Sea of Marmara. Marine Geology, 329–331, 58–74. https://doi.org/10.1016/j.margeo.2012.09.002